DOI 10.1007/s10334-004-0062-8

RESEARCH ARTICLE

Michael S. Hansen
Christof Baltes
Jeffrey Tsao
Sebastian Kozerke
Klaas P. Pruessmann
Peter Boesiger
Erik M. Pedersen

Accelerated dynamic Fourier velocity encoding by exploiting velocity-spatio-temporal correlations

Received: 1 June 2004
Revised: 12 August 2004
Accepted: 13 August 2004
Published online: 9 November 2004

M. S. Hansen (✉) · C. Baltes
J. Tsao · S. Kozerke
K. P. Pruessmann · P. Boesiger
Institute for Biomedical Engineering,
Swiss Federal Institute of Technology
(ETH), University of Zurich,
Zurich, Switzerland
E-mail: msh@mr.au.dk
Tel.: +45-89-495263
Fax: +45-89-496004

M. S. Hansen · E. M. Pedersen
Aarhus University Hospital,
Brendstrupgaardsvej,
8200 Aarhus N, Denmark

J. Tsao
Novartis Institutes of
BioMedical Research Inc.,
Cambridge, Mass., USA

Abstract *Objective:* To describe how the information content in a Fourier velocity encoding (FVE) scan can be transformed into a very sparse representation and to develop a method that exploits the compactness of the data to significantly accelerate the acquisition. *Materials and Methods:* For validation, fully sampled FVE datasets were acquired in phantom and in vivo experiments. Fivefold and eightfold acceleration was simulated by using only one fifth or one eighth of the data for reconstruction in the proposed method based on the *k-t* BLAST framework. Reconstructed images were compared quantitatively to those from the fully sampled data. *Results:* Velocity spectra in the accelerated datasets were comparable to the spectra from fully sampled datasets. The detected peak velocities remained accurate even at eightfold acceleration, and the overall shape of the spectra was well preserved. Slight temporal smoothing was seen in the accelerated datasets. *Conclusion:* A novel technique for accelerating time-resolved FVE scan is presented. It is possible to accelerate FVE to acquisition speeds comparable to a standard time-resolved phase-contrast scan.

Keywords Magnetic resonance imaging · Cine · Blood flow velocity · Pulsatile flow · Fourier analysis

Introduction

Phase-contrast velocity mapping [1] has been demonstrated to be a powerful tool for quantifying blood flow in the cardiovascular system [2, 3]. An extension of this method is Fourier velocity encoding (FVE) [4, 5] which acquires a velocity spectrum for each image pixel. The FVE technique uses flow-sensitive bipolar gradients to vary the first-order gradient moment in a stepwise manner, thereby encoding velocity in a similar fashion to that in which spatial location is encoded with standard phase-encoding gradients. The velocity spectrum is then recovered from the data by applying inverse Fourier transform along the velocity-encoded dimension.

Fourier velocity encoding has certain advantages over a simple phase-contrast measurement. For example, with a phase-contrast measurement, echo-time and signal-to-noise constraints often make it impossible to increase the spatial resolution sufficiently to resolve detailed features of the velocity distribution. In contrast, since FVE resolves the velocity distribution for each voxel, it is less susceptible to the partial volume effect [6]. The achievable echo time is often shorter for FVE, since the first-order moment increases quadratically with the duration of the gradient, while the amount of phase encoding (zeroth-order moment) only increases linearly. These features make FVE more suitable for accurate volume flow measurements and peak velocity determination [7]

in cases where there may be insufficient spatial resolution to resolve signal components at different velocities, e.g. for measuring peak flow through stenotic valves. In spite of these advantages, FVE is not widely used. This is mainly due to the long acquisition time associated with encoding one or more extra dimensions in *k*-space. Several techniques have been suggested for speeding up the FVE acquisition, but the speed is usually gained at the expense of either spatial [7, 8] or velocity [9] resolution.

In a typical FVE measurement, only a portion of the FOV contains flow information (e.g. blood vessels). For time-resolved flow quantification, an even smaller portion will exhibit time-varying changes. As a result, the signals will be confined to limited regions in space, velocity and time. Therefore, in principle, it is not necessary to acquire the full dataset and to resolve all spatial positions at all velocities and all time points. Intuitively, if a pixel at a certain spatial position, velocity, and time point is known to have no signal, the acquisition can be accelerated by skipping this pixel. However, the situation is more complicated in practice, since the raw MR data are acquired in the inverse (i.e. Fourier transform) domain. Thus, alternative ways of exploiting this redundancy is needed in order to accelerate the scan.

In dynamic imaging, new techniques have been developed which exploit spatio-temporal correlations in the data to accelerate the acquisition. Examples of such techniques include UNFOLD [10], TSENSE [11], *k-t* BLAST [12] and *k-t* SENSE [12]. In this paper, we propose to accelerate FVE by extending the approach of *k-t* BLAST. In particular, we make use of the insight of Twieg et al. [13], who showed that velocity encoding can be considered as an additional axis of *k*-space. As a result, an FVE acquisition with three encoded dimensions (two spatial and one velocity) is similar to a standard three-dimensional (3D) acquisition. In this work, it is demonstrated that by treating the velocity dimension in a similar fashion to a spatial dimension, we can apply the *k-t* BLAST technique to significantly accelerate a time-resolved FVE scan. Moreover, the present study examines the signal distribution in the FVE data space. This reveals that the FVE data space can have an even more compact representation compared to that of a time-resolved 3D scan, thus making time-resolved FVE scans particularly suitable for accelerated acquisition.

With the proposed method, it is shown that a FVE can be accelerated to the point that acquisition time is comparable to a standard phase-contrast scan. At the same time, the accelerated FVE scan retains the advantage of resolving detailed velocity information, while a phase-contrast scan can only determine the mean velocity within each image pixel. This advantage is particularly important at low to moderate spatial resolutions, where each voxel may contain spins at different velocities. Measurements were performed in a flow phantom and the results were verified in vivo data.

Theory

The principles of FVE have been described in detail elsewhere [4, 5], and only the necessary notation is reviewed here. For simplicity, we consider a 2D imaging experiment, but the general framework can be extended to an arbitrary number of dimensions in a straightforward fashion. In this simplified experiment, we consider only one pixel column at a frequency-encoded position. For that pixel column, there is one spatial (x, phase-encoding dimension) and one velocity (v) dimension. The signal equation is:

$$s(k_x, k_v, t) = \iint \rho(x, v, t) \mathrm{e}^{-\mathrm{i}2\pi(k_x x + k_v v)} \mathrm{d}x \, \mathrm{d}v \,, \qquad (1)$$

where $\rho(x, v, t)$ is the imaged object as a function of space x, velocity v and time t. k_v and k_v are the positions in *k*-space [13] along the spatial and velocity dimensions as determined by the encoding gradients, respectively. In the rest of this paper, time t refers to "cardiac phase". To image time-varying flow, the experiment needs to sample the k_x-k_v-t space sufficiently to reconstruct these signals at a given resolution and field of view along the spatial, temporal, and velocity directions. The coverage of this signal space is often time consuming, since in the simplest case, the acquisition of each point would require a repetition of the MRI experiment (i.e. lasting one repetition time, TR). After acquisition, the data are reconstructed through an inverse Fourier transform along k_x and k_v into x-v-t space. The typical FVE data from a phantom experiment are shown in Fig. 1. The upper row shows an image of the phantom on the left and the time-resolved velocity spectra at low (middle) and high (right) flow rates. The bottom row shows 3D isosurface renderings of the signals in x-v-t space and the corresponding signals in x-v-f space. The latter is obtained by applying inverse Fourier transform along time t. The isosurfaces in (Fig. 1) illustrate where most of the signal is contained, but there are also signals at lower intensities outside the surfaces. By transforming the data to x-v-f space (lower right), the representation becomes more concentrated in localized regions. The compact representation of data illustrates that the raw data in k_x-k_v-t space contain considerable spatial-velocity-temporal correlation, which can be exploited to accelerate the acquisition by utilizing the unoccupied regions in x-v-f space more fully.

The present work is based on the observation that the x-v-f space is analogous to the y-z-f space in 3D *k-t* BLAST [14], where the second spatial dimension is now replaced by a velocity dimension. Thus, in an analogous fashion,

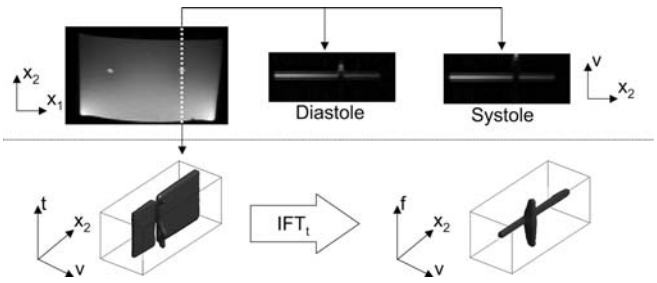

Fig. 1 Typical FVE dataset from a phantom experiment. Phantom consists of solid agarose with two parallel tubes. The *upper left panel* shows the summed intensity over all encoded velocity intervals. Frequency- and phase-encoding directions are denoted x_1 and x_2, respectively. The velocity spectra are shown for a frequency-encoding position passing through the center of the right tube at low and high flow rates, simulating diastole and systole, respectively. An isosurface representation of the same data in *x-v-t* space is shown on the lower left, and the corresponding but sparser *x-v-f* space is shown on the lower right

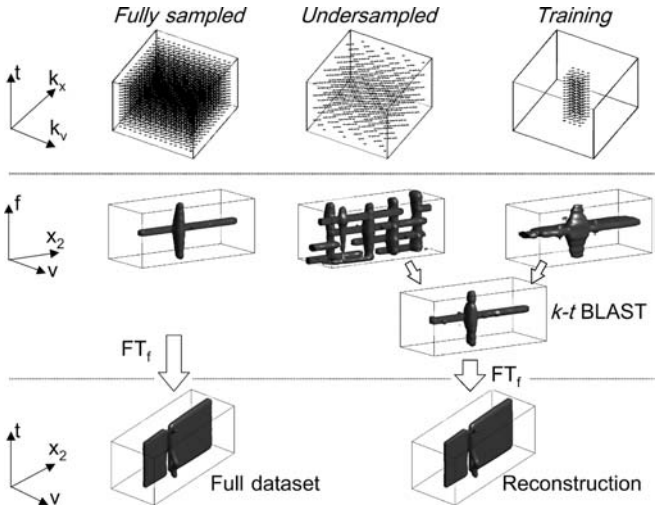

Fig. 2 The reconstruction process. The *top row from left to right* illustrates the sampling patterns for a full sampled dataset (for comparison), an undersampled dataset (acceleration factor 4), and a training dataset. The *second row* illustrates the concentration of signals in *x-v-f* space for the same frequency-encoded position as in Fig. 1. The *x-v-f* space for the fully sampled case (*left*) is identical to the one shown in Fig. 1, while the undersampled case (*middle*) shows fourfold aliasing, and the training data (*right*) is blurred due to the low spatial and velocity resolutions. The undersampled and training data are used in *k-t* BLAST reconstruction to yield the reconstructed *x-v-f* space shown in the *third row*, which is then Fourier transformed along temporal frequency *f* to yield the reconstructed *x-v-t* space in the *bottom row*. The reconstruction process is repeated for every frequency-encoded position

the acquisition can be accelerated through undersampling of the reciprocal k_x-k_v-t space, which introduces aliasing in *x-v-f* space. This undersampling and aliasing is illustrated in Fig. 2. The k_x-k_v-t space sampling patterns for the fully sampled and the undersampled cases (acceleration factor 4) are shown in the first two columns of the top row. The resulting signals in *x-v-f* space are illustrated in the middle row. It can be seen that, in the undersampled case, the signals are replicated (i.e. aliased) in *x-v-f* space. In other words, each pixel in the aliased *x-v-f* space receives signal contribution from multiple source locations. This aliasing process can be described as an encoding process whereby a vector of pixels $\boldsymbol{\rho}$ is mapped onto an aliased point ρ_{alias}. The aliasing is then resolved according to the reconstruction formula for *k-t* BLAST, as described in Tsao et al. [12]:

$$\boldsymbol{\rho} = \underline{\boldsymbol{\rho}} + \boldsymbol{\Theta} E^{\mathbf{H}} \left(\mathbf{E}\boldsymbol{\Theta}\mathbf{E}^{\mathbf{H}} + \psi \right)^{+} \left(\rho_{\text{alias}} - \mathbf{E}\underline{\boldsymbol{\rho}} \right) \tag{2}$$

where $\underline{\boldsymbol{\rho}}$ denotes a baseline estimate of $\boldsymbol{\rho}$. $\boldsymbol{\Theta}$ denotes the signal covariance matrix $\left\langle \left(\boldsymbol{\rho} - \underline{\boldsymbol{\rho}} \right) \left(\boldsymbol{\rho} - \underline{\boldsymbol{\rho}} \right)^{\mathbf{H}} \right\rangle$, $\mathbf{E} = \mathbf{1} = 1$ [1 ... 1] is the encoding matrix, and ψ is the noise variance. Superscript **H** indicates the complex conjugate transpose and superscript + indicates the Moore–Penrose pseudoinverse. In practice, the signal covariance matrix $\boldsymbol{\Theta}$ is not known exactly, so it is estimated from a set of training images as described in Tsao et al. [12]. In the case of FVE, the training images are obtained with low spatial and velocity resolutions to speed up acquisition. An example of the sampling pattern and *x-v-f* space of such a training dataset is shown in the last column of Fig. 2. The effect of reconstructing the data with (2) is illustrated in the lower half of Fig. 2. The reconstruction process is carried out for each frequency-encoded position separately. Figure 3 illustrates the reconstruction process in a more familiar velocity spectrum representation, which is analogous to what is shown in Fig. 2.

Materials and methods

Volume flow calculation

The mean velocity for each voxel was calculated as a weighted average in the following expression, using a phasor representation to account for the periodic boundaries of the Fourier-encoded velocity axis:

$$\bar{v}(\mathbf{x}) = \angle \left(\sum_{j=-N/2}^{N/2-1} \mathrm{e}^{\mathrm{i}\pi \frac{v_j}{v_{\max}}} \cdot \left| f\left(\mathbf{x}, v_j\right) \right| \right) \cdot \frac{v_{\max}}{\pi} \tag{3}$$

where $v_j = \frac{j}{N/2} v_{\max}$ denotes the *j*'th velocity, $v_{\max}$ is the encoding velocity, $\left| f(\mathbf{x}, v_j) \right|$ is the magnitude of the velocity spectrum at the *j*'th velocity at position $\mathbf{x}$, and N is the total number of encoded velocities. It should be noted that any linear scaling of the intensities, such as from inhomogeneous coil sensitivities, does not affect the average velocity, due to the phasor representation. The volume flow at each cardiac phase was then calculated by integrating the velocity over the vessel of interest at the corresponding time frame.

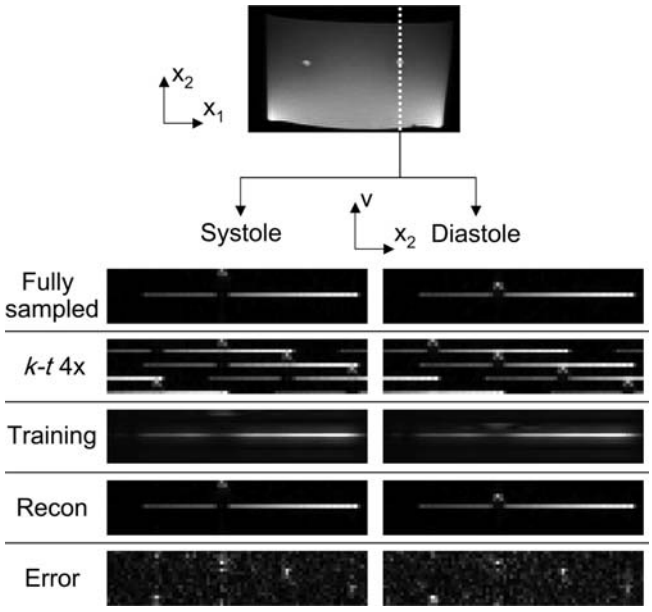

Fig. 3 The reconstruction process illustrated in the velocity spectrum representation. The *two columns* represent a systolic (*left*) and a diastolic (*right*) frame at the position indicated by the *dotted line* in the *top*. *Each row* illustrates the velocity spectrum for different data sets. From *top to bottom*: the fully sampled data for comparison, the undersampled data (acceleration factor 4), the low-resolution training data, the reconstruction result, and the difference between the fully sampled and the reconstructed result (scaled to reveal details)

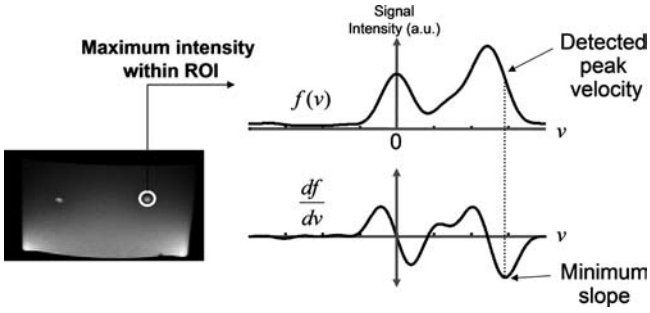

Fig. 4 Peak velocity detection procedure. The *left panel* shows an image of the phantom. The ROI is indicated by a *white circle*, encompassing the tube on the right side. The maximum-intensity-projected (MIP) velocity spectrum, denoted as $f(v)$, is obtained from the ROI, and is shown in the *upper right panel*. The derivative of the MIP spectrum, denoted as df/dv, is shown on the *lower right panel*. The peak velocity is selected as the minimum of the spectrum derivative

Peak velocity determination

For a vessel of interest, the peak velocity was determined with a technique modified from Galea et al. [7]. Firstly, a region of interest (ROI) encompassing the vessel was selected. A maximum intensity projection was then performed within this ROI along the spatial dimensions onto the velocity axis. In other words, for each velocity component the intensity was set to the maximum intensity among all spatial positions. This results in a single velocity spectrum for each time point. It should be noted that, since the vessel diameter was small, any spatial variation of the coil sensitivities across the vessel could be neglected in the maximum intensity projection. The peak velocity at each time point was selected from the corresponding velocity spectrum as illustrated in Fig. 4. The spectral peak at the highest velocity was selected. To avoid selecting peaks that were due to truncation artifacts from the low velocity resolution, the selection only included spectral peaks above a pre-chosen threshold. In the present study, the threshold was chosen to be 50% of the maximum spectrum intensity. This value was found to work robustly with all the examined datasets. The peak velocity was then identified as the velocity at the steepest point of the spectral peak, i.e. where the derivative of the spectrum attains a local minimum. An alternative approach to selecting the peak velocity is to choose the point where the velocity spectrum falls below a given threshold. However, the location of this point is affected to a large degree by the point spread function along the velocity dimension. The steepest-decent approach is potentially less dependant on the point spread function [7].

In vitro experiments

In vitro experiments were performed with an agar phantom containing embedded tubes (5 mm diameter) as illustrated in Fig. 1. A pulsatile flow (mean flow 10 ml/s) waveform was generated in the tubes using an UHCD MR flow system [15] (Quest Imaging, London, ON, Canada). The dimensions of the tubes and the mean flow were chosen to mimic the conditions in the common carotid artery. A gradient-echo FVE sequence was implemented on a Philips Intera 1.5 Tesla (Philips Medical Systems, Best, Netherlands) whole-body scanner. A 2D fully sampled FVE dataset was acquired with a matrix size of 128×76, a FOV of $179\times106\,\text{mm}^2$, a slice thickness of 8 mm, 16 velocity encoding steps, 32 time frames, an echo time of 5.6 ms, a repetition time of 8.5 ms, a flip angle of 15°, and an encoding velocity ($v_{\max}$) of 100 cm/s. From this fully sampled dataset, subsets of the data were used to simulate different acceleration factors and different amounts of training data.

The amount of training data needed to ensure good reconstruction quality was investigated. This issue has been investigated previously for the case of time-resolved anatomic imaging [16]. In that work, it was found that approximately 8–10 profiles (i.e. *k*-space lines) were needed to achieve an appropriate balance between low reconstruction error and a short duration for acquiring the training data. In this work, the requirements along the velocity encoding axis was investigated. The fully sampled in vitro dataset was decimated using an optimal sampling pattern as described in [17] to simulate eightfold acceleration. *k-t* BLAST reconstruction was then performed with various amounts of training data from no profiles up to all profiles. The amount of training was varied independently in both spatial and velocity-encoding directions. The relative RMS reconstruction error was calculated as follows:

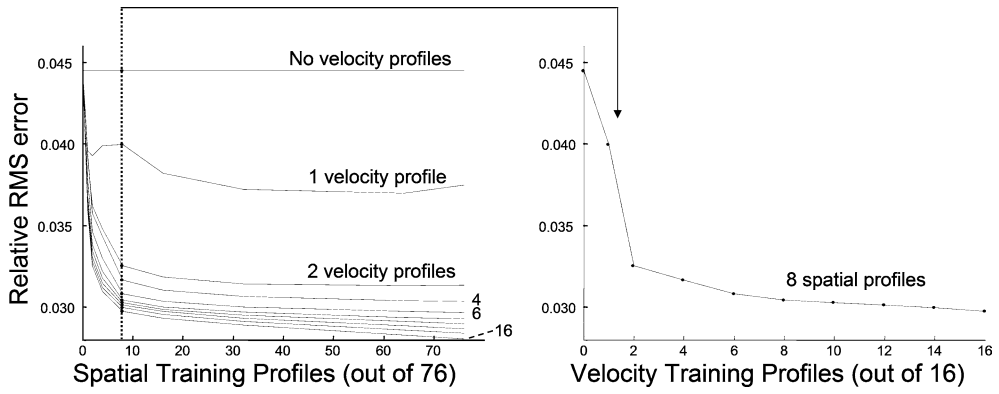

Fig. 5 Relative RMS reconstruction error (calculated according to (4) using different amounts of training data. In the *left panel*, each *curve* shows the effect of various numbers of training data profiles along the spatial dimension, while keeping the number of profiles along the velocity dimension constant. The *right panel* illustrates the effects of various numbers of profiles along the velocity dimension while keeping the number of profiles along the spatial dimension constant at eight profiles. Only one curve is shown on the *right panel* to avoid visual clutter

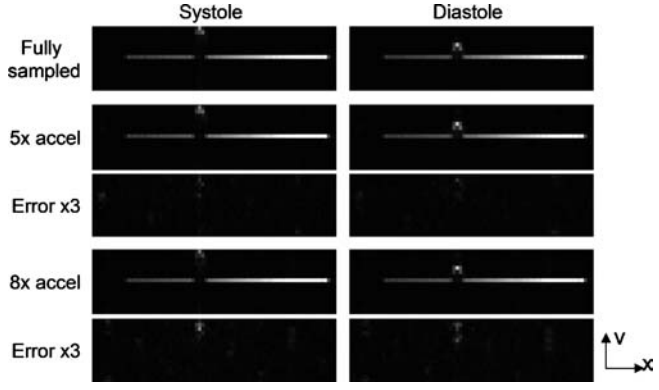

Fig. 6 Examples of velocity spectra from the in vitro experiment. The velocity spectra represent a "systolic" (*left column*) and a "diastolic" (*right column*) time frame for a frequency-encoded position passing through the center of one of the tubes in the agar phantom, as indicated by the *dotted lines* in Figs. 1 and 3. The *top row* shows the fully sampled dataset. The *middle two rows* show the results for fivefold acceleration and the corresponding reconstruction error, amplified three times to reveal difference. The *bottom two rows* show the results for eightfold acceleration

$$E_{\mathrm{RMS},t} = \sqrt{\frac{\sum_{i,j} \left| r_{i,j,t} - o_{i,j,t} \right|^2}{\sum_{i,j} \left| o_{i,j,t} \right|^2}} \qquad (4)$$

where $E_{\mathrm{RMS},t}$ denotes the relative RMS error at time frame t; $r_{i,j,t}$ and $o_{i,j,t}$ denote the i'th pixel value at the j'th velocity and time frame t in the reconstructed and original images, respectively. The summation was performed over all pixels and all velocities. The reported RMS error was then averaged over the entire pulsatile cycle. From these results, the suitable amount of training data was chosen, and this amount was fixed for all subsequent experiments.

To examine the effects of acceleration, the reconstructed images at fivefold and eightfold acceleration were compared with the images from the fully sampled data. Quantitative measures such as the peak velocity and the volume flow were evaluated.

In vivo experiments

Fully sampled FVE datasets were acquired in the common carotid artery of two healthy volunteers. The imaging plane was angulated perpendicular to the main flow direction, based on an in-flow angiographic image. The position of the slice plane was approximately 15 mm upstream from the carotid bifurcation. The parameters for the FVE scan were similar to those in the in vitro experiments, except for the following: in-plane resolution of 1.2–1.4 mm^2, and an encoding velocity of 130 cm/s. The reconstructed images at fivefold and eightfold acceleration were compared with the images from the fully sampled data in the same manner as for the in vitro experiments.

Results

In vitro experiments

Figure 5 shows the effects of different amounts of training data. In general, the reconstruction error dropped rapidly with very few profiles in the training data. Above 8–10 profiles in the spatial direction, there was only marginal additional reduction in reconstruction error. The results also show a similar trend for the velocity-encoding direction. Based on these results, it was chosen to use nine training data profiles in both spatial and velocity-encoding directions in the subsequent experiments.

A comparison of the in vitro reconstruction results is shown in Fig. 6. Qualitatively, the velocity spectra appeared similar among the fully sampled and accelerated cases. The reconstruction error was amplified in the figure to reveal the differences. There was some reconstruction error around the spectral peak, indicating that the reconstruction was unable to fully resolve the unaliased signals.

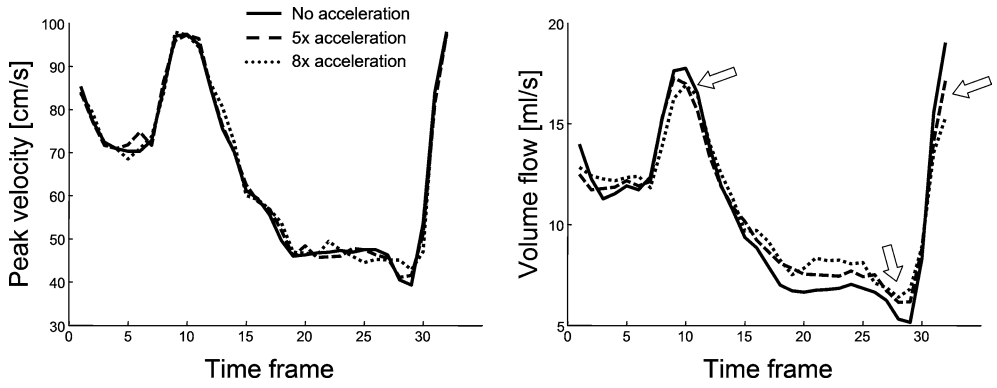

Fig. 7 Peak velocity (*left panel*) and volume flow (*right panel*) results for the in vitro experiment. The *solid, dashed* and *dotted lines* represent the fully sampled (i.e. no acceleration), and fivefold and eightfold accelerated cases, respectively. Volume flow was calculated from the velocity spectrum data according to (3)

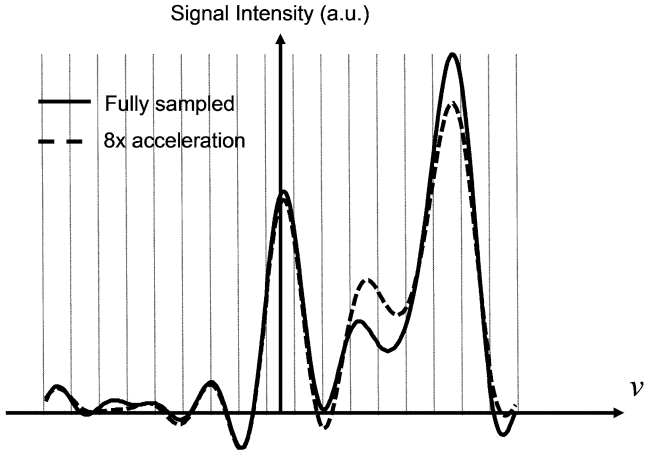

Fig. 8 Peak velocity spectra at a systolic frame from a single voxel experiencing partial volume effects in the in vitro experiment. The *two curves* illustrate the velocity distributions from the fully sampled (*solid line*) and the eightfold accelerated (*dashed line*) reconstructions. The curves are sinc interpolated. Only 16 velocity steps were encoded (indicated by the *light grid lines*). The high-velocity component is slightly attenuated in the accelerated case

The determined peak velocities and volume flow values are shown in Fig. 7 for the fully sampled, and fivefold and eightfold accelerated cases. Acceleration had minor effects on the detected peak velocities (Fig. 7, left panel), but the volume flow curves exhibited slight temporal low-pass filtering, resulting in some under- and over-estimation of the maximum and minimum volume flow values, respectively. (See arrows in Fig. 7, right panel). It should be mentioned that the gate delay was set suboptimally in this experiment. Consequently, the "systolic" peak occurred at the very last time frame. With the acquisition time gap due to gating, there was a temporal discontinuity between the first and last time frames. This created a more challenging situation than usual for the *k-t* BLAST method, which relies on a Fourier transform along the temporal dimension. As a result, a rather large volume flow error was seen for the accelerated cases at the last time frame.

To explore the low-pass temporal filtering of the volume flow curves further, Fig. 8 shows an example of velocity spectra from a single voxel containing both stationary and moving tissue at a systolic time frame. While the fully sampled and accelerated velocity spectra were qualitatively similar, slight attenuation of the high-velocity components was seen in the accelerated case. This attenuation resulted from incomplete unaliasing for the time-varying signal component. The time-averaged volume flow remained accurate, and it was determined to be 10.5, 10.7 and 10.8 ml/s for the fully sampled, and fivefold and eightfold accelerated cases, respectively. Additionally, since the location of the high-velocity peak was preserved, the peak velocity was practically unaffected by the acceleration (Fig. 7, left panel).

In vivo experiments

Example velocity spectrum images, and peak velocity and volume flow measurements for volunteers are shown in Fig. 9 and Fig. 10, respectively. The observations were similar to those for the in vitro experiments. The velocity spectra are qualitatively similar among the fully sampled and accelerated cases (Fig. 9). In the amplified reconstruction error images, it was possible to identify some reconstruction error around the spectral peaks. The volume flow curves exhibited some temporal low-pass filtering in the accelerated cases (Fig. 10), while the time-averaged volume flow measurements were similar among the fully sampled and accelerated cases. For all three cases, the time-averaged volume flow was determined to be between 10.1 and 10.3 ml/s for volunteer 1, and between 9.5 and 9.7 ml/s for volunteer 2. Acceleration had little effect on the peak velocity measurement, but slight overestimation was seen for diastole (see arrows in Fig. 10, left column).

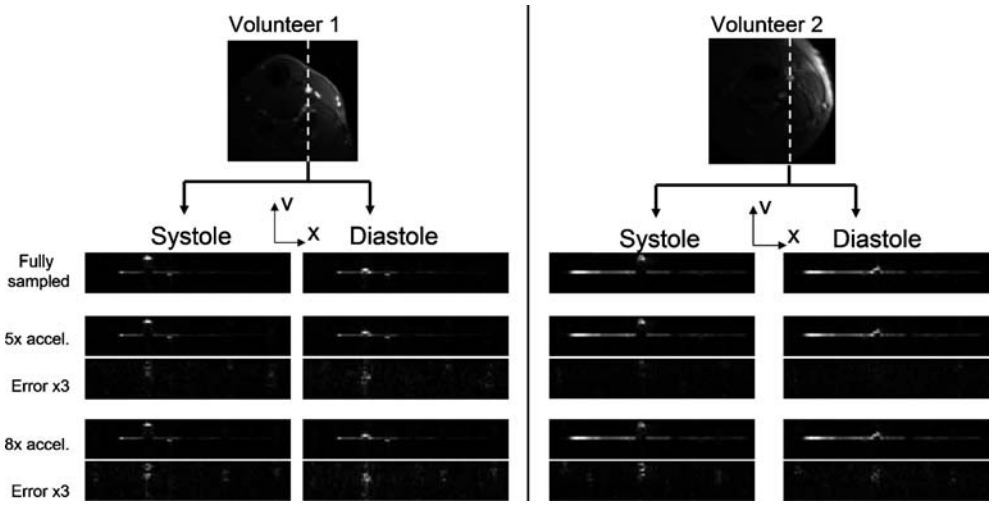

Fig. 9 Reconstruction results from two volunteers. The *upper row* shows a cross section of common carotid artery. For the frequency-encoded position indicated by the *dotted line*, the velocity spectra from a systolic (high-flow) and diastolic (low-flow) time frame are shown for each of the two volunteers. The *second row* shows the fully sampled dataset. The *next two rows* show the results for fivefold acceleration and the corresponding reconstruction error, amplified three times to reveal difference. The *bottom two rows* show the results for eightfold acceleration

Discussion

This paper demonstrates that the data in a typical FVE acquisition can be transformed into a much more compact representation, indicating that fewer degrees of freedom are needed to describe such a data set, thus opening up the possibility for significant acceleration. It is shown that the previously presented *k-t* BLAST framework can be used for accelerating time-resolved FVE scans if the velocity-encoding direction (or directions) is treated in a similar fashion to a spatial dimension. For example, the standard 2D FVE acquisition with one velocity encoding dimension can be treated in a similar manner to an acquisition with three spatially encoded dimensions [14].

Through simulations with in vitro experiments, it was shown that *k-t* BLAST reconstruction of accelerated FVE datasets is possible. The appropriate amount of training data in terms of balancing between low reconstruction errors and short acquisition time was found to be 8–10 training data profiles in the spatial encoding direction. This was in accordance with previous findings [16]. For the velocity direction, a smaller number of profiles seemed to be sufficient, but we chose nine profiles to err on the safe side.

The acceleration led to some alterations in the velocity spectra, although the typical error was difficult to see unless it was amplified. The main effect was that the volume flow curve exhibited some temporal low-pass filtering. The degree of the low-pass filtering became more pronounced with increasing acceleration. This dependence on acceleration was expected, since fewer degrees of freedom could be recovered when fewer data were acquired. Since the reconstruction equation of *k-t* BLAST minimizes the expected reconstruction error, higher temporal frequencies, which typically have lower signal intensities, may be traded for lower temporal frequencies, resulting in the low-pass filtering effect observed. In practice, the extent of low-pass filtering can be reduced either by using lower acceleration factors or by using *k-t* SENSE [12] to take advantage of the complementary information provided by multiple receiver coils.

The overall shape of the velocity spectra was generally well preserved. Accordingly, the peak velocities could be determined rather accurately, even at high accelerations. Other measures of the velocity spectrum should also be relatively insensitive to the acceleration. These include the time-averaged volume flow, and the mode of the velocity spectrum (i.e. the most common velocity component as determined by the algorithm of Bittoun et al. [9]). This renders the proposed method particularly suitable for applications that rely on such measures for quantification. Examples include peak velocity determination downstream of stenotic vessels and heart valves. Peak velocity determination in the evaluation of stenosis is of clinical importance [18], but the detection of peak velocity is not reliable with a standard phase-contrast sequence due to intra-voxel averaging, which occurs unless very high spatial resolution is used. Normally, the need to encode the velocity dimension would make the acquisition time prohibitively long. This would make a breathhold acquisition impossible. In the case of vessel stenosis (e.g. in the carotid artery), this would increase the overall examination time to the extent that the scan becomes very susceptible to patient movement during the acquisition. Thus, the proposed method provides a unique means of addressing such clinically relevant questions. Additionally, since

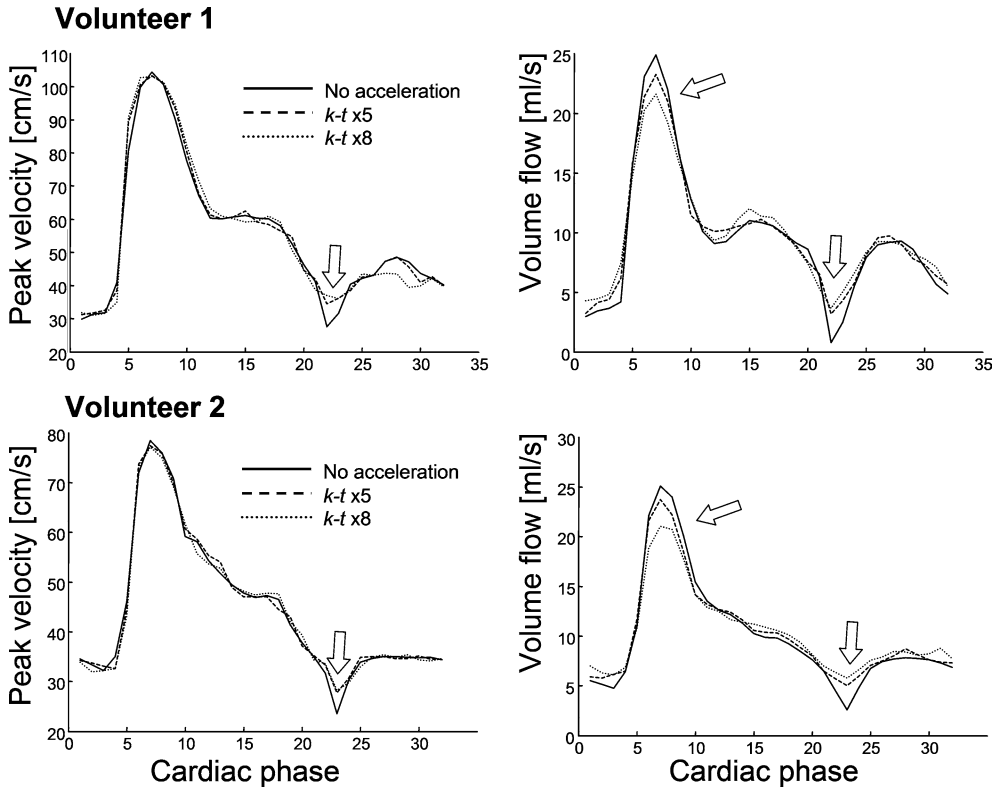

Fig. 10 Determination of peak velocity (*left column*) and volume flow (*right column*) for volunteers 1 (*top row*) and 2 (*bottom row*). The *solid, dashed* and *dotted lines* represent the fully sampled (i.e. no acceleration), and fivefold and eightfold accelerated cases, respectively. Volume flow was calculated from the velocity spectrum data according to (3)

the mean volume flow is well preserved at high acceleration factors, the proposed method is suitable for determining mean volume flow in situations, where the FOV contains both very high and very low flow rates, such as for simultaneous measurements of both arterial and venous vessels.

The accelerated datasets presented here were obtained by simulation from fully sampled datasets. This situation is similar but not identical to an accelerated acquisition. In the latter case, larger *k*-space distances are traversed between each encoding step, potentially leading to more complicated eddy current effects, which need to be taken into account in order to avoid artifacts [14].

It should be mentioned that when accelerating acquisition by as much as a factor of 8, the training data acquisition takes a relatively long time compared to the undersampled acquisition. For one of the examples shown here, the training data contains 42% of the number of profiles in the undersampled acquisition at acceleration factor 8, resulting in a net acceleration factor of 5.6. However, since training data can be acquired in a separate acquisition without much penalty [16], it is still possible to take advantage of the high acceleration factors in breathhold situations by acquiring the undersampled and training data in two separate breathholds. Also, the acquisition time for the training data can be reduced by using fewer velocity profiles, and by utilizing parallel imaging.

The main advantage of the presented method over previous methods for accelerating FVE is that it provides the acceleration without explicitly sacrificing spatial or velocity resolution. The high acceleration factors demonstrated here allow acquisition of FVE datasets in a time frame comparable to a standard phase-contrast scan with only slight temporal blurring. Thus, the technique holds considerable promise for FVE scanning under time constraint, e.g. in breathhold acquisition or in situations where patient movement is difficult to control for an extended period. Furthermore, the suggested approach can also be extended in a straightforward fashion when more spatial and velocity dimensions are encoded. The extension to additional spatial and velocity encoding dimensions is likely to make the FVE data space even more sparse, which would render it very suitable for high accelerations. FVE of multiple velocity dimensions could be useful in situations where flow patterns are complex (but non-turbulent), with significant in-plane components. In such cases, one-directional FVE would only partially help in resolving all velocity components.

Conclusion

A novel method for acceleration of FVE has been presented. Using this method, it is possible to accelerate FVE to acquisition speeds that are comparable to a standard phase-contrast scan. The acceleration is gained without compromising spatial or velocity resolution, and the overall shape of the reconstructed velocity spectra is generally well preserved in the accelerated datasets. Some temporal smoothing is seen in the accelerated datasets, but the unique abilities of the FVE acquisition to detect peak velocities is uncompromised despite the significant reduction of scan time.

Acknowledgements MSH would like to acknowledge support from the Danish Heart Foundation, grant#02-2-3-43-22021. This work was also supported by the SEP Life Sciences grant TH7/02-2 of the ETH Zurich, and Philips Medical Systems, Best, The Netherland. Jeffrey Tsao is a recipient of a postdoctoral fellowship from the Canadian Institutes for Health Research.

References

1. Van Dijk P (1984) Direct cardiac NMR imaging of heart wall and blood flow velocity. J Comput Assist Tomogr 8(3):429–436
2. Szolar DH, Sakuma H, Higgins CB (1996) Cardiovascular applications of magnetic resonance flow and velocity measurements. J Magn Reson Imaging 6(1):78–89
3. Mohiaddin RH, Pennell DJ (1998) MR blood flow measurement. Clinical application in the heart and circulation. Cardiol Clin 16(2):161–187
4. Moran PR (1982) A flow velocity zeugmatographic interlace for NMR imaging in humans. Magn Reson Imaging 1(4):197–203
5. Redpath TW, Norris DG, Jones RA, Hutchison JM (1984) A new method of NMR flow imaging. Phys Med Biol 29(7):891–895
6. Tang C, Blatter DD, Parker DL (1993) Accuracy of phase-contrast flow measurements in the presence of partial-volume effects. J Magn Reson Imaging 3(2):377–385
7. Galea D, Lauzon ML, Drangova M (2002) Peak velocity determination using fast Fourier velocity encoding with minimal spatial encoding. Med Phys 29(8):1719–1728
8. Pat GT, Pauly JM, Hu BS, Nishimura DG (1998) One-shot spatially resolved velocity imaging. Magn Reson Med 40(4):603–613
9. Bittoun J, Bourroul E, Jolivet O, Idy-Peretti I, Mousseaux E, Tardivon A, Peronneau P (1993) High-precision MR velocity mapping by 3D-Fourier phase encoding with a small number of encoding steps. Magn Reson Med 29(5):674–680
10. Madore B, Glover GH, Pelc NJ (1999) Unaliasing by fourier-encoding the overlaps using the temporal dimension (UNFOLD), applied to cardiac imaging and fMRI. Magn Reson Med 42(5):813–828
11. Kellman P, Epstein FH, McVeigh ER (2001) Adaptive sensitivity encoding incorporating temporal filtering (TSENSE). Magn Reson Med 45(5):846–852
12. Tsao J, Boesiger P, Pruessmann KP (2003) $k-t$ BLAST and $k-t$ SENSE: dynamic MRI with high frame rate exploiting spatiotemporal correlations. Magn Reson Med 50(5):1031–1042
13. Twieg DB, Katz J, Peshock RM (1987) A general treatment of NMR imaging with chemical shifts and motion. Magn Reson Med 5(1):32–46
14. Kozerke S, Tsao J, Razavi R, Boesiger P (2004) Accelerating cardiac cine 3D imaging using $k-t$ BLAST. Magn Reson Med 52(1):19–26
15. Frayne R, Holdsworth DW, Gowman LM, Rickey DW, Drangova M, Fenster A, Rutt BK (1992) Computer-controlled flow simulator for MR flow studies. J Magn Reson Imaging 2(5):605–612
16. Hansen MS, Kozerke S, Tsao J, Pruessman KP, Boesiger P, Pedersen EM (2004) Influence of training data quality on *k-t* BLAST reconstruction. In: Proceedings of 12th Annual Meeting ISMRM, Kyoto
17. Tsao J, Kozerke S, Hansen MS, Boesiger P, Pruessman KP (2004) Optimized canonical sampling pattern in *k-t* space with two and three spatial dimensions for *k-t* BLAST and *k-t* SENSE. In: Proceedings of 12th Annual Meeting ISMRM, Kyoto
18. Carpenter JP, Lexa FJ, Davis JT (1996) Determination of duplex Doppler ultrasound criteria appropriate to the North American Symptomatic Carotid Endarterectomy Trial. Stroke 27(4):695–699